Quantitative study of the destructive quantum-interference effect on coherent population trapping

E. Breschi,[1] G. Kazakov,[2] R. Lammegger,[3] G. Mileti,[1] B. Matisov,[2] and L. Windholz[3]

[1]*Laboratoire Temps-Fréquence, University of Neuchâtel, 2000 Neuchâtel, Switzerland*
[2]*St. Petersburg State Polytechnic University, St. Petersburg 195251, Russia*
[3]*Institute of Experimental Physics, TU–Graz, 8010 Graz, Austria*

We investigate experimentally and theoretically the coherent population trapping (CPT) effect occurring in ^{87}Rb D_1 line due to the interaction with linearly polarized laser light (lin∥lin CPT). In this configuration, the coherence is strongly influenced by the structure of the excited state; consequently, the quantum interference between dark states is an essential feature of this interaction scheme. We study the lin∥lin CPT resonance as a function of the laser optical detuning. The comparison between experimental and theoretical results allows us to quantify the contribution from different dark states to the total signal. Based on these results, we investigate the signal depending on both the pressure broadening of the optical transition and the laser linewidth, and we find in which conditions the laser linewidth does not degrade the lin∥lin CPT resonance.

I. INTRODUCTION

The first investigations of the coherent population trapping (CPT) effect were performed theoretically and experimentally in the 1970s [1–3]. In accordance with these early works, the CPT effect is due to a coherence between ground states caused by the interaction with a quasiresonant, two-frequency, and coherent light field. CPT and related effects (such as electromagnetically induced Transparency [4] and absorption [5]) have an impact on both the atomic system state and the light beam propagation through the media.

CPT resonances with a narrow linewidth can be recorded in the simplest case in quantum systems with two long-lived ground states and one excited state coupled by a dichromatic coherent light field. In this configuration, the quantum system is prepared in a nonabsorbing state (the dark state). The energy levels in such a configuration are arranged similar to the greek letter Λ (so-called Λ system) and can be found, for instance, in alkali atoms. In the experiment, CPT resonances are recorded by varying the frequency difference of two spectral electromagnetic field components around the value of the frequency splitting of the ground states. The properties of the CPT resonances can be exploited in a wide range of applications such as atomic magnetometry [6], atomic frequency standards [7], pulse delaying, and compression for optical memory [8].

The problem in the use of CPT effect in those applications is its low strength. Often the dark state induces only a small variation in the light transmitted through the atomic sample. To overcome this limitation, recently several novel light-atom interaction schemes were proposed [9–14]. In particular, in work [15] the authors show that a significant enhancement of the CPT effect can be obtained in the so-called lin∥lin CPT configuration. Here two copropagating linearly polarized laser waves with parallel linear polarization vectors are resonant with the transitions to $5^2 P_{1/2}$ $F_e=1$ of the ^{87}Rb isotope. A detailed analysis of the two-photon Λ transition process shows that in a lin∥lin CPT configuration, the CPT resonance depends critically on the excited-state hyperfine

structure (HFS) [16], in a way different to that of the well-known CPT resonance obtained by a circularly polarized laser field [17]. In the case of circularly and linearly polarized laser field, the dark state arises from a vectorial ($\Delta m_F=0$) and quadrupolar coupling ($\Delta m_F=2$), respectively.

A theoretical study of four-level system describing the CPT resonance depending on the structure of the ground and excited atomic levels has been published in [18]. The interest of these systems relies to the possibility of controlling its optical properties via the quantum interference arising between two dark states, for instance, by means of the phases of the laser fields [19,20] or the local phase of the dark states [21]. In the present work, we study the behavior of the lin∥lin CPT resonance occurring within the manifold of the hyperfine transitions of the ^{87}Rb D_1 line. In our case, the CPT resonance depends on the structure of the excited hyperfine states and it is described in detail in Sec. II with the model developed for the data interpretation. We analyze the lin∥lin CPT resonances as a function of the laser detuning and the homogeneous broadening (in Sec. IV), which depends on the pressure broadening (due to the buffer gas in the cell) and the laser linewidth. Note that the evaluation of the laser linewidth influence on the dark states is crucial for applications and has not been investigated much so far. A theoretical study of the laser linewidth effects on CPT resonance for achieving selective excitation of atoms (with application in laser cooling and quantum computing) is presented in Ref. [22]; while in [23], the author has demonstrated with his model a scheme that allows large time delay for large bandwidth optical pulse.

We perform our studies with two different light sources: a pair of phase-locked (PL) extended cavity diode lasers (ECDLs) and a current modulated vertical cavity surface emitting diode laser (VCSEL). The PL ECDLs have, in good approximation, pure dichromatic fields with a narrow linewidth. On the contrary, the modulated VCSEL has a multi-frequency spectrum with broader linewidth. A detailed discussion of the laser sources and the experimental setup is presented in Sec. III.
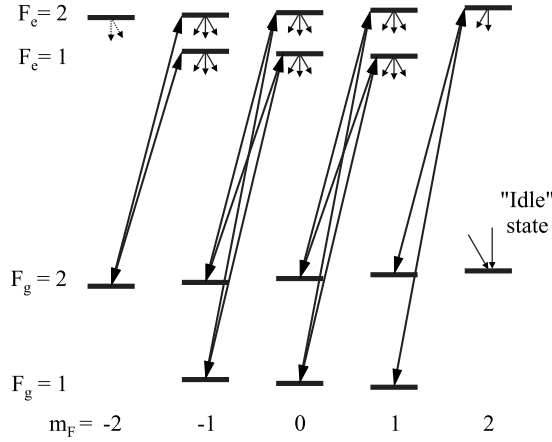
FIG. 1. Schematic diagram of the light-induced transitions giving the σ^+-σ^+ CPT resonance by excitation of the HF transitions belonging to the D_1 line of the ^{87}Rb isotope. The Λ system involving the ground states $|F_g=1, m_F=0\rangle$ and $|F_g=2, m_F=0\rangle$ gives rise to the (often called) 0-0 CPT resonance which is used as reference in atomic clocks. The atomic population is partially collected in the state $|F_g=2, m_F=2\rangle$ via an optical-pumping process. For this reason, the state $|F_g=2, m_F=2\rangle$ is called as *idle state*. The small arrows represent the spontaneous decay of excited states.

A. Application of the lin∥lin CPT resonance in compact atomic clocks

In the last years, many efforts have been steered into the realization of compact CPT-based atomic clocks [24]. The CPT excitation scheme usually used is based on the interaction of Cs or Rb atoms with a circularly polarized laser field, i.e., either σ^+ or σ^- transitions are induced by the two-frequency components of the driving laser field (in the following called σ-σ CPT). A typical excitation scheme in case of the manifold of hyperfine transitions within the ^{87}Rb D_1 is illustrated in Fig. 1. Here, a weak magnetic field of few tens of μT oriented in laser propagation direction is applied to lift the degeneracy of the Zeeman sublevels. In this paper, we will discuss the same atomic system in case of lin∥lin excitation, and the scheme of the interaction is represented in Fig. 3.

In this σ-σ configuration, the resonance used as reference in frequency standard applications is the coherent superposition of the sublevels $|F_g=1, m_F=0\rangle$ and $|F_g=2, m_F=0\rangle$ being on the first order not sensitive to magnetic fields. The problem of this interaction scheme relies on the fact that the state $|F_g=2, m_F=2\rangle$ is not involved in the excitation process. As a consequence, the optical-pumping effect caused by the isotropic spontaneous decay of the excited states accumulates the population into this *idle state* which, thus, represents a loss mechanism for the clock reference resonance. This leads (especially at higher laser intensities and low buffer gas pressure) to a reduced signal-to-noise ratio because most of state population is concentrated in those Zeeman sublevels with highest (lowest) m_F quantum numbers.

On the contrary, in case of a lin∥lin CPT configuration (discussed in Sec. II), no idle states are present and the state population is concentrated symmetrically around the Zeeman sublevel with quantum number $m_F=0$. This can be under-

stood qualitatively because there is no transfer of net angular momentum from the linear polarized light to the atoms in the excitation process. Thus a better signal-to-noise ratio is expected especially in the case of higher laser intensities and low buffer gas pressures. This characteristic makes the lin∥lin CPT resonance a valid candidate for high performance compact atomic clock (a detailed study is presented in [25]).

II. MODEL AND INTERACTION SCHEME

A model based on the density-matrix approach has been used for the data interpretation and has been described in detail in Refs. [26,27]. Here we report on the basic approach and we give an intuitive picture of the results essential for our discussion.

Let us to consider a ^{87}Rb atom excited by a two-frequency laser field resonant to HF transitions $5\,^2S_{1/2}$ $F_g=1, 2 \leftrightarrow 5\,^2P_{1/2}$ $F_e=1$ of the D_1 line. For such a system, the density-matrix evolution is given by

$$\dot{\rho}_{ij} = -\frac{i}{\hbar}\sum_k [H_{ik}\rho_{kj} - \rho_{ik}H_{kj}] + \sum_{k,l} \Gamma_{ij,kl}\rho_{kl}. \quad (1)$$

The Hamiltonian $\hat{H}$ has two terms: the atomic unperturbed Hamiltonian $\hat{H}_0$ and the interaction operator $\hat{V}$, i.e., $\hat{H} = \hat{H}_0 + \hbar\hat{V}$. $\Gamma_{ij,kl}$ is the relaxation matrix element describing the relaxation processes.

The two-frequency laser field can be written as follows:

$$\vec{E}(z,t) = \sum_{j=1,2} \left[\frac{\vec{E}_j}{2} \exp\{i[\omega_j t + \varphi_j(t) - k_j z]\} \right] + \text{c.c.}, \quad (2)$$

whereas the laser linewidth is modeled by the phase fluctuations $\varphi_j(t)$.

The absorbed laser power in an optically thin gas cell (weak absorption) can be calculated by

$$\Delta P = \rho_{exc} \hbar \omega_{opt} \gamma N_a, \quad (3)$$

where ρ_{exc} is the total excited-state population, ω_{opt} is the optical transition frequency, γ is the excited-state relaxation rate, and N_a is the number of active atoms taking part in the excitation process. In an optically thin gas cell, due to a weak absorption, ρ_{exc} is not a function of the optical path because the matrix elements of the interaction Hamiltonian $\hbar V_{ij}$ are assumed to be constant along the optical path. At high temperatures, the gas cell becomes optically thick. The consequence is that the density-matrix elements (and with them the dark states) are functions of the light intensity along the optical path. Modeling of such a coupled behavior is rather complicated because, strictly speaking, the effects of propagation determined by the Maxwell equations are strongly coupled with the density-matrix equations of the quantum system. Our experiments are performed with an optically thick ^{87}Rb vapor cell. Therefore, in the model the optical path is divided in a set of subsequent parts. Assuming constant electrical fields (E_i=const) in each thin layer, the density matrix is calculated. Finally, the Maxwell equations for the slowly varying E-field amplitude and phase [28] are used

to calculate the variations in the E fields within the layer. Thereafter, the density matrix of the next layer is determined by using the new E field derived from the previous layer. This procedure is repeated for all subsequent parts. In the numerical calculations, we do not take into account modifications of the transverse intensity distribution. Nevertheless, this simple phenomenological approach allows us to reproduce the experimental results (see Sec. IV). In the following, the ground and excited-state Zeeman sublevels are called g, g', and e, respectively. Note that g and g' belong to different hyperfine ground states and a dark state can be created when the two transitions $|g\rangle \leftrightarrow |e\rangle$ and $|g'\rangle \leftrightarrow |e\rangle$ are excited simultaneously. If the laser field intensity is much lower than the saturation limit for each optical transition and the cell is optically thin, the total excited-state population ρ_{exc} is proportional to the light power absorbed [cf. Eq. (3)]. Neglecting fast oscillating terms $\sim O(\omega_i + \omega_j)$ and $\sim O(2\omega_j)$, etc. (rotating wave approximation), the excited-state density-matrix element is connected to the ground-state density-matrix elements via

$$\rho_{exc} = \sum_{e,g,g'} \left\{ \frac{V_{eg}^0 V_{g'e}}{\gamma' \gamma} [G_{ge} + G_{g'e} + i(F_{ge} - F_{g'e})]\rho_{gg'} \right\}$$
(4)

and the ground-state matrix elements can be derived from the following set of equations:

$$\dot{\rho}_{gg'} = -i\rho_{gg'}(\omega_{gg'} - \omega_g + \omega_{g'}) + \Gamma\left(\frac{1}{8}\delta_{gg'} - \rho_{gg'}\right)$$

$$- \sum_{g'',e}\left[\frac{V_{ge}V_{eg''}}{\gamma'}(G_{g'e} + iF_{g'e})\right]\rho_{g''g'}$$

$$- \sum_{g'',e}\left[\frac{V_{g''e}V_{eg'}}{\gamma'}(G_{ge} - iF_{ge})\right]\rho_{gg''} + \frac{\delta_{gg'}}{8},$$
(5)

$$\sum_{e,g'',g'''}\left\{ \frac{V_{g''e}V_{eg'''}}{\gamma'}[G_{g''e} + G_{g'''e} + i(F_{g'''e} - F_{g''e})] \right\},$$

$$\sum_g \rho_{gg} = 1.$$
(6)

Here $\hbar V_{ij}$ are the matrix elements of the interaction Hamiltonian (Rabi frequencies) in the frame rotating with the corresponding laser frequency component; γ' is the decay rate of the optical coherence ρ_{eg}; and $\delta_{gg'}$ is the Kronecker delta. ω_g is the frequency of laser component interacting with the level g and $\omega_{gg'}$ is the frequency spacing between the levels $|g\rangle$ and $|g'\rangle$. The ground-state relaxation rate denoted by Γ depends on the temperature of the cell, type, and pressure of buffer gas, geometry of the cell, the laser power, and the geometry of laser beam [29]. In our simulation, Γ is the free fit parameter in our simulation which is estimated from the measurements.

In [30], the authors demonstrate that the optical coherence decay rate γ' is determined by the laser linewidth Γ_L, by the spontaneous relaxation rate γ_{sp} which is for the state $5^2 P_{1/2}$
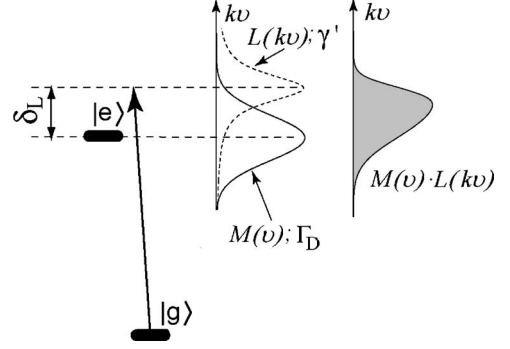

FIG. 2. Schematic view of the homogeneous broadening profile [Lorentzian curve $L(kv)$ of linewidth γ' in dashed line] of a transition ($|g\rangle \leftrightarrow |e\rangle$). δ_L^{eg} is the laser detuning. The Gaussian curve (of linewidth Γ_D) in solid line represents the Doppler profile $M(v)$ of the transition. In Eq. (8), G_{eg} is proportional to the gray area under the product of the two curves [$L(kv)M(v)$].

of $^{87}\text{Rb} \simeq 2\pi \times 5.6$ MHz, and by the pressure broadening γ_c which depends on the type of buffer gas and on the buffer gas pressure in the cell,

$$\gamma' = \frac{\gamma_{sp} + \gamma_c + \Gamma_L}{2}.$$
(7)

To understand the physical meaning of γ', let us consider a generic single transition $|g\rangle \leftrightarrow |e\rangle$. The excitation of this transition by a laser light field of linewidth Γ_L results in a homogeneous broadened profile that can be described with a Lorentzian curve of linewidth γ' (Fig. 2). In a buffer gas cell, the collisional rate is large; therefore, it is necessary to account for the changes in the atomic velocities along the laser beam propagation direction. We derived Eqs. (4) and (5) under the hypothesis that the Rabi frequencies V_{ij} are much smaller than the frequency of velocity changing collisions. As a consequence, these equations are averaged over the atomic velocities along the laser field propagation direction. This fact appears in the expressions for coefficients G_{ge} and F_{ge} in Eqs. (4) and (5); G_{ge} and F_{ge} are real and equal to

$$G_{ge} = \int_{-\infty}^{+\infty} \frac{(\gamma')^2 M(v)}{(\gamma')^2 + (\delta_L^{eg} - kv)^2}dv,$$

$$F_{ge} = \int_{-\infty}^{+\infty} \frac{\gamma'(\delta_L^{eg} - kv)M(v)}{(\gamma')^2 + (\delta_L^{eg} - kv)^2}dv,$$
(8)

where $M(v)$ is the atomic velocity distribution and δ_L^{eg} is the laser detuning. The coefficient G_{ge} is proportional to the strength of the single optical transition $|g\rangle \leftrightarrow |e\rangle$; while the coefficient F_{ge} allows to calculate the shift of the resonance frequency. For our intent, we focus our attention to the coefficient G_{ge} which is schematically represented in Fig. 2. G_{ge} is proportional to the gray area delimited by the product of two profiles: the Doppler profile represented by a Gaussian curve $M(v)$ of linewidth Γ_D and the homogeneous profile represented by a Lorentzian curve $L(kv)$ of linewidth γ'. If
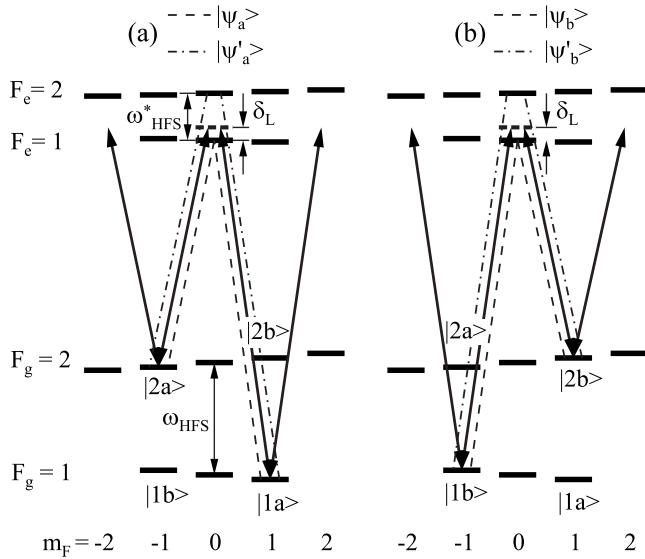
FIG. 3. Schematic diagram of the light-induced transitions giving the lin‖lin CPT resonance at $\omega \approx \omega_{HFS}$ to compare with Fig. 1. The levels involved are $|1a\rangle = |F_g=1, m_F=+1\rangle$ and $|2a\rangle = |F_g=2, m_F=-1\rangle$ part (a) of the figure; $|1b\rangle = |F_g=1, m_F=-1\rangle$ and $|2b\rangle = |F_g=2, m_F=+1\rangle$ part (b) of the figure. In the presence of a low magnetic field along the laser propagation direction (=quantization axis) the dark states in (a) and (b) are degenerate. The solid arrows are representing the components of the exciting laser field and δ_L is the laser detuning.

different $|g\rangle \leftrightarrow |e\rangle$ transitions are excited, G_{ge} characterizes the contribution of each transition to the total excitation process.

Now, we extend the previous consideration made for a single optical transition to a dark state. The necessary condition for creating the dark state is that the transitions from both ground states $|g\rangle$ and $|g'\rangle$ toward the same excited level $|e\rangle$ are simultaneously excited by two coherent electromagnetic field components, i.e., the relative frequency jitter of the electromagnetic field components is negligible. This condition is fulfilled either in the VCSEL or in the PL ECDLs (see Sec. III). The straightforward consequence is that the one-photon detuning of both light field components must coincide ($\delta_L^{eg} = \delta_L^{eg'}$). Under this condition, from Eq. (8) the relation $G_{ge} = G_{g'e} = G_e$ can be derived. In synthesis, the G coefficient for a general dark state depends only on the excited states involved (and not on the ground states). When different dark states occur simultaneously, the contribution to the total signal of each single dark state can be characterized by calculating G_e. Our model takes into account the Zeeman and hyperfine structure of the ^{87}Rb atoms. In the following, we define the interaction scheme, i.e., which group of atomic sublevels are involved in the dark state preparation. Finally, we present the results obtained by applying the model to an isolated reduced system, in order to show how the G_e coefficients describe the CPT-resonance strength.

Figure 3 shows the relevant transitions induced by the coherent σ^+ and σ^- components of the linearly polarized light fields expressed in spherical tensor basis. In Fig. 3, we do not report the σ^+-σ^+ and σ^--σ^- groups of transitions. In general, the existence of a CPT resonance is directly con-
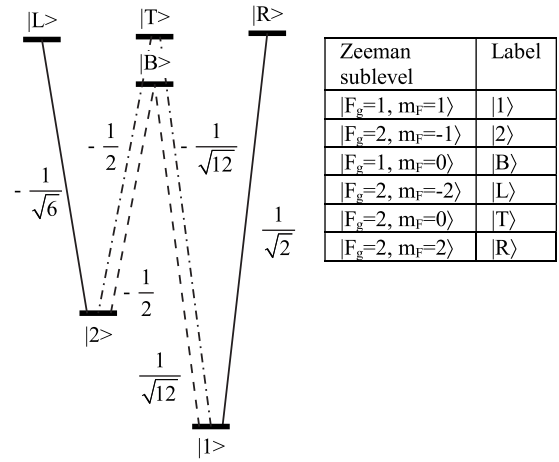

FIG. 4. Isolated six-level excitation system. The coefficients reported near the transition are proportional to the Rabi frequencies V_{eg}, i.e., they are the dipole matrix element for the transitions expressed as multiples of the coefficient $V^0 = \sqrt{\frac{3\gamma_{sp}c^3\hbar}{2\omega^3}}$.

nected via the phase relation between the Rabi frequencies (phase relation of laser fields and atomic wave functions) of each transition of the Λ–scheme [19]. In the specific case of lin‖lin excitation, the dark states arising from the σ^+-σ^+ and σ^--σ^- are orthogonal; thus, they interfere destructively and do not contribute to the CPT resonance at $\omega \approx \omega_{HFS}$ [9].

We study the σ^+-σ^- transitions between ground-state Zeeman sublevels with $m_F = \pm 1$. The feature of the CPT resonance is related with the presence of two excited levels ($F_e = 1, 2$), both allowed for dipole transitions. In synthesis, four dark states contribute to the lin‖lin CPT resonance at $\omega \approx \omega_{HFS}$: $|\Psi_a\rangle$ and $|\Psi_b\rangle$ are the coherent superpositions of the Zeeman sublevels $|1a\rangle \leftrightarrow |2a\rangle$ and $|1b\rangle \leftrightarrow |2b\rangle$ through the excited state $F_e = 1$, while $|\Psi_a'\rangle$ and $|\Psi_b'\rangle$ are the coherent superpositions of the same Zeeman sublevels via the excited state $F_e = 2$. When a magnetic field is applied along the quantization axis, $|\Psi_a\rangle$-$|\Psi_b\rangle$ and $|\Psi_a'\rangle$-$|\Psi_b'\rangle$ split with a factor of ± 28 Hz/μT determined by the nuclear g factor. Remark that the transitions toward the outermost Zeeman sublevels $|F_e=2, m_F= \pm 2\rangle$ play an important role in the formation of the dark state $|\Psi_a'\rangle$ and $|\Psi_b'\rangle$, as we are going to show in next paragraph.

A. Simplified atomic system: Analytical solution

To point out how the G_e coefficients can describe the lin‖lin CPT resonance, we apply the approach presented at the beginning of this section to Fig. 3(a), under the hypothesis that the six levels participating to the interaction are isolated. Similar considerations can be applied to Fig. 3(b) and then to the lin‖lin CPT resonance. Figure 4 is the diagram of the isolated six-level system. The Zeeman sublevels are named with a short label for handling with a compact notation. The coefficients reported near each transition are the dipole matrix elements expressed as multiples of $V^0 = \sqrt{\frac{3\gamma_{sp}c^3\hbar}{2\omega^3}}$. These coefficients are proportional to the Rabi frequencies V_{eg} [31,32]. For instance, in our notation the Rabi frequency for the transition $|1\rangle \leftrightarrow |R\rangle$ is named V_{1R} and

is equal to $(\frac{1}{\sqrt{2}} \frac{V^0 E_1^+}{2\hbar})$, where E_1^+ is a circularly polarized component of $\vec{E}_1$.

There are only two ground state not degenerate ($|1\rangle$ and $|2\rangle$), in our simplified scheme; therefore, the normalization condition (6) in the regime of low laser field intensities ($I_{las} \ll I_{sat}$) gives $\rho_{11} + \rho_{22} \simeq 1$. There are two excited states; thus $e = 1, 2$ such as for $e = 1$ the excited state has one sublevel $|B\rangle$ and for $e = 2$ the excited state has three sublevels $|L\rangle$, $|T\rangle$, and $|R\rangle$. We introduce for simplicity the new variables: f (population difference), R and J (real and imaginary part of ρ_{12}),

$$\rho_{11} = (1 + f)/2, \quad \rho_{22} = (1 - f)/2, \quad \rho_{12} = R + iJ. \quad (9)$$

The total excited-state population ρ_{exc} can be obtained by applying Eq. (4),

$$\rho_{exc} = \frac{1}{\gamma}[W + (W_1 - W_2)f + 4W_{12}R]. \quad (10)$$

From Eqs. (5) and (9), we obtain the set of equations for variables f, R, and J,

$$\dot{f} = -(\Gamma + W)f - 4D_{12}J + W_2 - W_1,$$

$$\dot{R} = -(\Gamma + W)R + (\Omega - \Delta)J - W_{12},$$

$$\dot{J} = D_{12}f - (\Gamma + W)J - (\Omega - \Delta)R. \quad (11)$$

Here $\Omega = (\omega_2 - \omega_1 - \omega_{21})$ is the Raman detuning and Γ is ground-state relaxation rate. W is the so-called "optical-pumping rate" and the quantity Δ is a measure for the light shift of the microwave transition (i.e., the shift of ω_{21}, i.e., the frequency difference between $|1\rangle$ and $|2\rangle$ in Fig. 4). Following our notation, we obtained:

$$W_1 = \frac{|V_{1B}|^2}{\gamma'}G_1 + \frac{|V_{1T}|^2 + |V_{1R}|^2}{\gamma'}G_2, \quad (12)$$

$$W_2 = \frac{|V_{2B}|^2}{\gamma'}G_1 + \frac{|V_{2T}|^2 + |V_{2L}|^2}{\gamma'}G_2, \quad (13)$$

$$W = W_1 + W_2, \quad (14)$$

$$W_{12} = \frac{V_{1B}V_{B2}}{\gamma'}G_1 + \frac{V_{1T}V_{T2}}{\gamma'}G_2, \quad (15)$$

$$D_{12} = \frac{V_{1B}V_{B2}}{\gamma'}F_1 + \frac{V_{1T}V_{T2}}{\gamma'}F_2, \quad (16)$$

$$\Delta = \frac{|V_{2B}|^2 - |V_{1B}|^2}{\gamma'}F_1 + \frac{|V_{2T}|^2 + |V_{2L}|^2 - |V_{1T}|^2 - |V_{1R}|^2}{\gamma'}F_2, \quad (17)$$

where G_1 and G_2 are the G coefficients for $e = 1, 2$ determined by applying Eq. (8) to the simplified six-level scheme. Substituting the stationary solution of the set of Eqs. (11) into Eq. (10), we obtain the following analytical expression for the total excited-state population:

$$\rho_{exc} = \frac{1}{\gamma}\left[W - \frac{(W_1 - W_2)^2 + 4W_{12}^2}{\Gamma + W} \right.$$
$$\left. + \frac{4[D_{12}(W_1 - W_2) - W_{12}(\Omega - \Delta)]^2}{(\Gamma + W)[(\Gamma + W)^2 + 4D_{12}^2 + (\Omega - \Delta)^2]}\right]. \quad (18)$$

The first two terms in Eq. (18) do not depend on the two-photon detuning Ω; the third term gives the change in the absorption due to the CPT effect. Finally, we substitute the Rabi frequencies (V_{eg}) into Eqs. (12), (13), and (15) and we get

$$W_1 = \frac{|V^0|^2}{\gamma'}\left[\frac{1}{12}G_1 + \frac{7}{12}G_2\right], \quad (19)$$

$$W_2 = \frac{|V^0|^2}{\gamma'}\left[\frac{3}{12}G_1 + \frac{5}{12}G_2\right], \quad (20)$$

$$W_{12} = \frac{|V^0|^2}{\gamma'}\frac{G_2 - G_1}{4\sqrt{3}}. \quad (21)$$

When $G_1 = G_2$, the two terms $(W_1 - W_2)$ and W_{12} are vanishing; therefore, the third term in Eq. (18) is vanishing and the CPT resonance goes to zero. This is evidence of destructive quantum interference between the different dark states prepared through the two excited-state hyperfine sublevels.

In this section, we summarize a method for calculating the CPT resonance based on the fact that the light power absorbed by the atoms is proportional to the detected signal and can be calculated by using Eqs. (3)–(5). On the basis of a simplified six-level system, we showed analytically that the excited-state hyperfine structure of ^{87}Rb plays an important role in the CPT excitation process due to a destructive quantum-interference effect. It is found that the characteristic of this interference can be well described by the ratio G_1/G_2 determined by the laser detuning δ_L and the optical coherence decay rate γ'. A ratio close to unity expresses similar (excitation) strengths in both dark states, which leads to a high degree of interference and to a cancellation of the CPT resonance.

III. EXPERIMENTAL SETUP

A sketch of the experimental setup is shown in Fig. 5. The core is a glass cell with a volume of a few cm^3 containing the ^{87}Rb isotope and N$_2$ as buffer gas. In particular, two similar cells are used containing 0.5 and 1.5 kPa of buffer gas, respectively. The cell temperature during is stabilized to (68 ± 1) °C, corresponding to a Doppler broadening of $\Gamma_D = 2\pi \times 540$ MHz of the optical transitions. Since the light fields are both copropagating, the Doppler broadening of the CPT resonance is due to the 6.8 GHz difference frequency. Note that—in the case of a buffer gas cell—the microwave Doppler effect is strongly reduced by the Dicke narrowing [33] because the atoms are confined within a volume much smaller than the 4.4 cm wavelength, corresponding to the 6.8 GHz frequency. At a temperature of 68 °C, the ^{87}Rb cell becomes optically thick. Therefore, when a single mode laser (VCSEL or ECDL) is in resonance, the cell transmittance
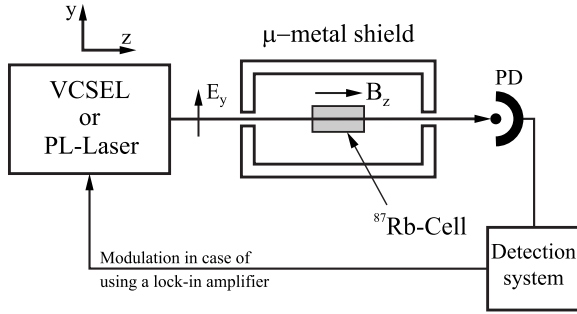
FIG. 5. Schematic block diagram of the experimental setup. Two laser light sources have been alternatively used during the experiments: a modulated VCSEL and two PL ECDLs. The detection system block consists of a current amplifier, a digital oscilloscope readout by a computer , and a lock-in amplifier (optional). E_y indicates the direction of the electrical field vector of the linearly polarized laser radiation. In the experiments, a magnetic field B_z =3 μT is applied in a laser propagation direction.

[i.e., the ratio between the laser intensity after and before the cell (I/I_0)] is always ≤ 0.3 corresponding to an optical thickness ≥ 1.

The laser radiation transmitted through the cell is collected onto a photodetector (PD) whose signal is amplified in a current amplifier afterward. Finally, the variation (increase) in the optical transmission is recorded by a digital oscilloscope directly connected to the current amplifier. Additionally, the CPT resonance can be monitored by using a lock-in amplifier.

In order to avoid the influence of spurious magnetic fields and magnetic gradients, the cell was inserted in a CO-NETIC alloy magnetic shield. Inside the shielding, a solenoid provided the longitudinal magnetic field B_z=$(3.0 \pm 0.2)\mu$T in order to lift the degeneracy of the Zeeman sublevels. The magnetic field has been regularly monitored during the experiments by using the g_J dependence of the outermost CPT resonance [15], i.e., the dark states created by the coherence of $|F_e=1, m_F=0\rangle$ and $|F_e=2, m_F=\pm 2\rangle$.

The functional block *VCSEL* or *PL laser* indicates that the experiments are performed either with a current modulated VCSEL or with *PL ECDLs*. Both laser systems have a Gaussian beam profile and a beam waist of 2 mm$(1/e^2)$. However, it is important to outline that the relevant difference between both laser systems is their spectral linewidth $\Gamma_V > 100 \Gamma_{PL}$. The characteristics of the two laser systems are shortly described in the following.

Modulated VCSEL (see Ref. [34]). The injection current of a single mode VCSEL emitting at 795 nm is directly modulated with 3.417 GHz (i.e., half of ground-state hyperfine separation in ^{87}Rb) with 10 dBm of rf power. The VCSEL has a broad spectrum; the measured linewidth is $\Gamma_V \approx 2\pi \times 100$ MHz. The modulation performance has been evaluated through the one-photon ^{87}Rb absorption spectrum by changing the frequency and the amplitude of the current modulation. We did not notice any influence of amplitude modulation, and the frequency modulation index was evaluated to be about 1.8. Under these conditions, about 68% of the total laser power is equally distributed in the first-order sidebands, which are used for the dark state excitation. The

remaining 32% of the total power is distributed among mainly the carrier frequency and the higher-order sidebands. These off-resonant parts of the VCSEL spectrum can cause one-photon excitation processes because of the Doppler broadening of the hyperfine transitions. Additionally, the not absorbed off-resonant light is increasing the dc and shot-noise levels of the photodetector.

PL lasers. The PL-laser system basically consists of two ECDLs called master and slave laser (both characterized by narrow spectrum, $\Gamma_{ECDLs} \approx 0.5$ MHz). The master laser is stabilized to the ^{87}Rb D_1 line $5^2 S_{1/2} F_g=2 \rightarrow 5^2 P_{1/2} F_e=1$ transition, using an auxiliary evacuated ^{87}Rb cell in a Doppler-free dichroich atomic vapor laser locking (DF-DAVLL) configuration [35,36]. Due to the high-speed servo loop for the laser stabilization, the linewidth of the master is reduced by a factor of 10. The slave laser is—via a heterodyne beat signal—phase locked to the master laser. Therefore, the light beams from the master and the slave laser are superimposed on a fast photodiode which detects the 6.8 GHz beat required for the experiments. After amplification, the heterodyne beat signal is down converted in a double balanced ring mixer to 50 MHz and is compared with a reference frequency signal stemming from an intermediate frequency (IF) oscillator. A phase/frequency detector provides an output signal proportional to the phase difference between the down-converted beat note and the IF oscillator. To close the feedback loop, the phase detector's output signal is fed back to the slave laser. In the setup, a combined analog-digital phase detector is used. In this way, a large capture range and a dead zone free locking is achieved simultaneously. The root-mean-square (rms) phase noise level (relative phase jitter) of the PL setup is $\Phi_{rms} \leq 50$ mrad (measured in the band of 1 Hz–1 MHz). As $\Phi_{rms} \ll \pi$ is well fulfilled, no degradation or additional broadening of the CPT resonance is observable [37]. In the case of PL ECDLs, the frequency components of the dichromatic electromagnetic field are separated by 6.835 GHz to bridge over the splitting of the ^{87}Rb hyperfine ground states. The intensities as well as the linear polarization state are selected to be the same for both frequency components. Finally, to avoid a residual broadening of the CPT resonances due to a wave-vector mismatch, a polarization maintaining single mode fiber is used to ensure perfect collinear wave vectors of the two-frequency components.

Figure 6 shows the photocurrent variation (top plot) and the lock-in signal (bottom plot) for a typical CPT resonance prepared with PL ECDLs. In our experiments, the CPT-resonance amplitude A_C is defined as the photocurrent variation relative to its background, and the CPT-resonance linewidth $\Delta \nu_C$ is the full width at half maximum (FWHM) of the resonance. We chose this definition of A_C [38] because we aim the quantitative study of quantum interference between dark states. Our approach allows to separate the strength of the CPT effect, which is affected by the quantum interference, and the light level in the experiments, which changes using PL ECDLs or VCSEL because of the contribution of the off-resonance frequencies in the modulated VCSEL spectrum. The role of the (background) light level—mainly determining the signal-to-noise ratio—in the experiments is very important for the applications and deserves to be stud-
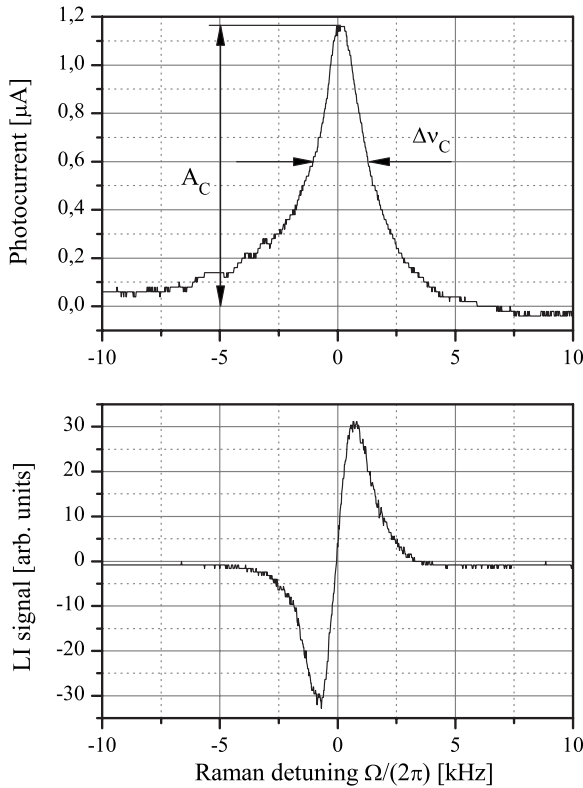
FIG. 6. An example of a typical CPT resonance prepared with PL ECDLs resonant with the group of transitions toward $F_e = 1$ (laser intensity equal to 3.8 mW cm^{-2}). Both the oscilloscope (top) and lock-in (bottom) signals are represented. The amplitude of the CPT resonance and its linewidths are $A_C = 1$ μA and $\Delta\nu_C = 3$ kHz, respectively. The variation in the normalized optical transmission due to the CPT is about 4%. Note that in the same condition with modulated VCSEL, we record about 3% of normalized optical transmission variation. The difference is due to the background light level increased by the presence of the off-resonance frequencies.

ied in detail separately. In accordance with the definitions given above, for the experimental conditions of Fig. 6 the normalized optical transmission due to the CPT effect is about 4% and 3% for PL ECDLs and modulated VCSEL, respectively.

IV. INFLUENCE OF EXCITED-STATE HFS ON THE lin∥lin CPT RESONANCE

The influence of the excited-state hyperfine structure of the ^{87}Rb D_1 line is evidenced by studying the lin∥lin CPT resonance versus the laser detuning (δ_L) in a cell containing ^{87}Rb and N$_2$ as buffer gas $P_{N_2} = 0.5$ kPa. The collisional broadening γ_c at this pressure is about $2\pi \times 70$ MHz [39], i.e., γ_c is almost 12 times smaller than the splitting of the hyperfine excited states ($\omega_{HFS} = 2\pi \times 17$ MHz). As a consequence, the hyperfine excited-state structure remains resolved.

These measurements can be easily performed with a modulated VCSEL since the VCSEL output frequency can be tuned with injection current over a wide frequency range
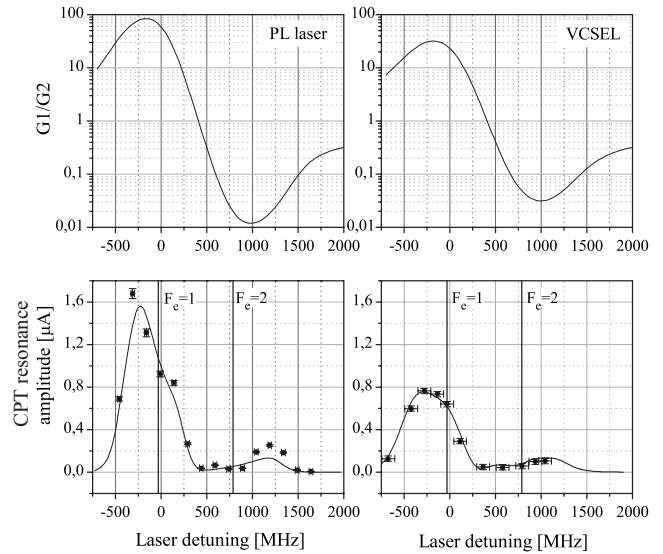

FIG. 7. The lower plots show the dependence of CPT-resonance amplitude (A_C) versus laser detuning (δ_L) in case of a total resonant laser intensity of 3.8 mW/cm^2, a temperature of 68 °C, and for a Rb cell with $P_{N_2} = 0.5$ kPa; while in the upper plots, the G_1/G_2 ratio (calculated for both cases) is reported. The maximum of absorption is marked by the vertical lines (the pressure shift is about −30 MHz). The value $\delta_L = 0$ is defined with respect to an evacuated ^{87}Rb cell. In both cases, A_C goes to zero when $(G_1/G_2) = 1$ and has two maxima at the maximum and the minimum of (G_1/G_2), respectively. Remark that the maxima of A_C are shifted with respect to the maxima of absorption in the cell.

(more than 10 GHz). The situation is different for the PL ECDLs. Here, the frequency of the master laser (i.e., the detuning δ_L) was determined via an ^{87}Rb saturation spectrum additionally overlapped by transmission fringes stemming from a cofocal Fabry-Perot interferometer with a free spectral range of $\nu_{FSR} = 149.85$ MHz. Therefore, a tuning range of about 2 GHz (within the HFS of the excited state $5^2 P_{1/2}$) with a frequency uncertainty of $\delta\nu \sim 5$ MHz is achieved with both laser system.

The dependence of the CPT-resonance amplitude (A_C) on δ_L is shown in the lower plots of Fig. 7, for experiments performed with PL ECDLs and modulated VCSEL, left and right columns, respectively. In Fig. 7, the points are the results of the experiments, while the solid lines are the model results obtained numerically by solving the coupled set of density-matrix and Maxwell equations with Γ as free fit parameter (see Sec. II). The value of the ground-state relaxation rate Γ is determined by fitting the CPT-resonance width $\Delta\nu_C$ obtained in the experiments. In case of the VCSEL source, a width $\Delta\nu_C = 1$ kHz and $\Delta\nu_C = 10$ kHz is measured for a laser detuning $\delta_L = 0$ (transitions toward $F_e = 1$) and $\delta_L = +2\pi \times 817$ MHz (transitions toward $F_e = 2$), respectively. As mentioned in [15], the CPT resonance arising from the group of transitions toward $F_e = 2$ is broader than the one arising from transitions toward $F_e = 1$. But, interestingly, negligible differences in the width $\Delta\nu_C$ are observed for CPT resonances prepared by the PL ECDL system.

To quantify the influence of each dark state contributing to the CPT resonance, in Sec. II the coefficients G_e have

been introduced. In the two upper plots of Fig. 7, the calculated (G_1/G_2) values are reported as a function of the laser detuning for the two sets of data. In each plot, $\delta_L = 0$ refers to the unperturbed group of transitions toward $F_e = 1$ (evacuated cell), and the dotted lines represent the maxima of absorption for $F_e = 1(\delta_L \approx -2\pi \times 30$ MHz) and $F_e = 2(\delta_L \approx +2\pi \times 787$ MHz) in the cell containing $P_{N_2} = 0.5$ kPa [collisional shift is (-22.2 ± 0.4) GHz K$(kPa)^{-1}$ [39]]. For each laser system, we observe that A_C shows two relative maxima which are both shifted with respect to the two maxima of absorption in the cell. In particular, the maxima of A_C coincide with the maximum and the minimum values of (G_1/G_2), respectively. Note that, in general, the dark state $|\Psi'_a\rangle$ is affected by the losses due to the one-photon transitions toward to the outermost excited levels $5^2 P_{1/2}$ $F_e = 2$, $m_F = \pm 2$ (see Fig. 3). For this reason when $(G_1/G_2) < 1$, the resulting lin∥lin CPT resonance is smaller than the one for $(G_1/G_2) > 1$ [15]. The values of A_C noticeably decrease when the light sources (PL ECDLs or VCSEL) are tuned between the two group of transitions. In fact we showed that the dark states prepared via different excited hyperfine sublevels interfere destructively, and, if their involvements into excitation process are equal, i.e., $G_1/G_2 = 1$, the CPT resonance vanishes. Similar effect has been discussed in the case of two Zeeman sublevels belonging to the same hyperfine manifold in [40], and in the case of two-photon absorption when both hyperfine excited states can be intermediate states [41]. Moreover, by comparing the left and right parts of Fig. 7, we can observe that the A_C maximum recorded in the experiments using PL ECDLs is larger than the A_C maximum obtained with the modulated VCSEL. The measured behavior of A_C vs δ_L is well reproduced by the model calculations. In particular—at the experimental conditions referring to Fig. 7—the G_e coefficients calculated for PL ECDLs are bigger than these coefficients calculated for the modulated VCSEL either for $e = 1$ and 2.

The behavior of the σ-σ CPT-resonance amplitude, width, and position as a function of the laser detuning δ_L is studied in a higher-pressured buffer gas cell (5.5 kPa of neon) by the authors in [42]. As anticipated in Sec. I, the dark states obtained by interactions with linearly and circularly polarized light fields are intrinsically different. In the case of circularly polarized light fields, the dark states arise from a vectorial coupling ($\Delta m_F = 0$) and no quantum interference occurs [16]. This different nature of the lin∥lin and σ-σ CPTs is shown in Fig. 8. Here, the master laser (determining the laser detuning δ_L) of the PL ECDLs is tuned at the crossover resonance between the transitions $F_g = 1 \leftrightarrow F_e = 1$ and $F_g = 1 \leftrightarrow F_e = 2$. In case of the lin∥lin CPT, the resonance amplitude A_C is strongly suppressed because both dark states—via the excited states $F_e = 1$ and $F_e = 2$—have equal strengths $G_1 = G_2$ and interfere destructively (cf. Fig. 7). Unlike, in the case of σ-σ CPT, such a destructive interference is not observable due to the specific phase relation of the Rabi frequencies.

A. lin∥lin CPT-resonance amplitude versus homogeneous broadening

The previous results allow us to predict the influence of the homogeneous broadening γ' [Eq. (7)] on the lin∥lin CPT
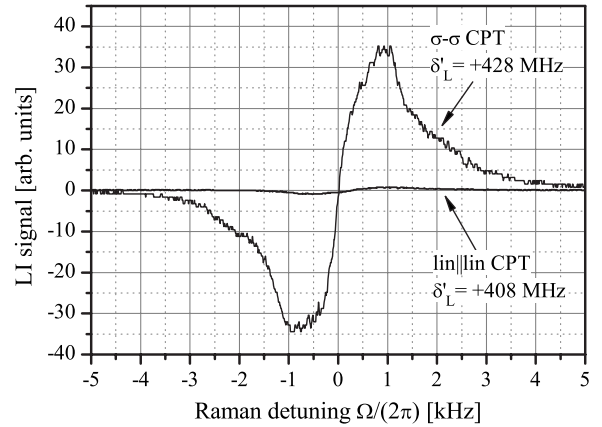

FIG. 8. Evidence of the different nature of dark state excited with circular and linear light field, σ-σ and lin∥lin CPT resonances, respectively. The two resonances are recorded under the same experimental conditions. In particular, the laser ($I = 3.8$ mW/cm^2) is tuned near by the cross-over resonance [$\delta'_L = \delta_L/(2\pi) = +408$ MHz] of the $5^2 P_{1/2}$ $F_e = 1$ and $F_e = 2$ states (evacuated ^{87}Rb cell). The lin∥lin CPT resonance is about 40 times weaker than the σ-σ one because of the destructive interference influence.

resonance. In practice, we compare the experiments performed with PL ECDLs and modulated VCSEL in a selected ^{87}Rb cells containing 0.5 kPa of N$_2$ for a fixed value of the laser detuning. In this section, we compare the dark state prepared with the two lasers systems in two ^{87}Rb cell with different relevant pressure N$_2$. In particular, we study the case of detuning $\delta_L = 0$, when the master laser of the PL ECDLs is stabilized. Under such conditions, a PL-laser linewidth Γ_P of $2\pi \times 0.04$ MHz is achieved, i.e., it is 2500 times narrower than the VCSEL linewidth ($\Gamma_V \approx 2\pi \times 100$ MHz). Figure 9 shows the CPT-resonance amplitude (A_C) versus the resonant laser power for ^{87}Rb cells with $P_{N_2} = 0.5$ kPa and $P_{N_2} = 1.5$ kPa [Figs. 9(a) and 9(b)], respectively. The main
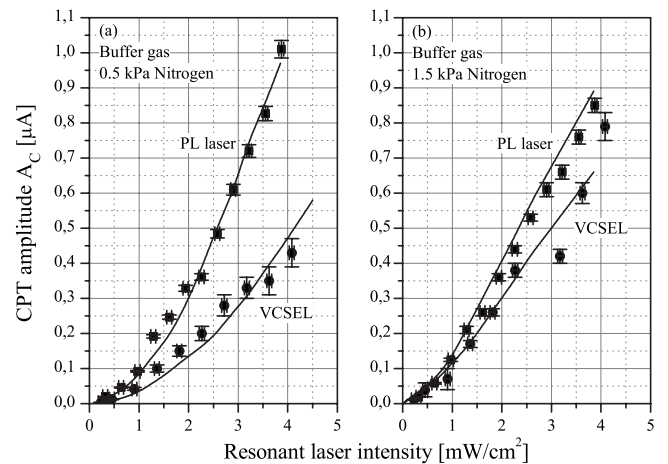

FIG. 9. Dependence of lin∥lin CPT-resonance amplitude (A_C) versus the resonant laser power for experiments performed in two cells such as (a) $P_{N_2} = 0.5$ and (b) $P_{N_2} = 1.5$ kPa. The solid points refer to experiments and the lines show the numerical calculations. Remark that in (a) there is a noticeably difference in A_C depending on the laser source, while in (b) that difference is reduced.

difference between the experiments performed with those cells is the relation of the collisional broadening in each cell and the VCSEL linewidth. For P_{N_2}=0.5 kPa, the collisional broadening contribution $\gamma_c=2\pi\times 70$ MHz is smaller than the linewidth of the VCSEL ($\gamma_c<\Gamma_V$). On the contrary, for P_{N_2}=1.5 kPa γ_c is $2\pi\times 210$ MHz, i.e., about two times of Γ_V. In both cases, γ_c is much bigger than the PL-laser linewidth ($\gamma_c\gg\Gamma_P$). In Figs. 9(a) and 9(b), the solid points refer to the experiments performed with the modulated VCSEL and the PL ECDLs, respectively. The solid lines show the results of the theoretical model (cf. Sec. II), which are in good quantitative agreement with the experimental results. We observe that the difference in A_C obtained with the two laser systems is large in (a) while it is reduced and almost negligible, for $I_L<1$ mW/cm^2, in (b). To explain the observed behavior, we first note that in Ref. [34], the authors showed a reduction in the CPT-resonance amplitude when the laser linewidth is larger than the pressure broadening for the dark states created via the interaction with circularly polarized laser light. They explained these results by considering that the dark state is excited in atoms belonging to several velocity classes. This argument is still valid, of course, in the case of lin‖lin excitation, but can only partially explain our results. In the previous parts of this paper, we have demonstrated that in the case of dark state arising from a quadrupolar coupling (Δm_F=2), the excited-state hyperfine structure must be taken into account for each δ_L. Under quadrupolar coupling conditions, the phase relations of all Rabi frequencies involved within the excitation scheme plays a major role. Using the formalism developed in our model, we can conclude that for intensities lower than the saturation of the optical transitions, when $\gamma_c>\Gamma_L$ [condition satisfied in Fig. 9(b)], it is possible to obtain the same (G_1/G_2) ratio for the two laser systems. It is possible, then, to find experimental conditions in which the amplitude of the lin‖lin CPT resonance A_C is independent of the laser linewidth. On the contrary, when $\gamma_c<\Gamma_L$ [condition satisfied in Fig. 9(a)], the laser linewidth plays an important role: the ratio (G_1/G_2) for

experiments with the modulated VCSEL is smaller than (G_1/G_2) for the PL ECDLs. We cannot appreciate the influence of the laser linewidth in the CPT linewidth (Δ_C). For both laser sources, Δ_C increases linearly with the laser intensity in the same range of values. The values of $\Delta\nu_C$ extrapolated to zero laser intensities are $\approx 2\pi\times 1.5$ kHz and $\approx 2\pi\times 0.8$ kHz for the cell with 0.5 kPa and 1.5 kPa buffer gas pressure, respectively, mainly caused by collisional broadening effects [43].

V. CONCLUSIONS

We present a study the CPT resonance prepared in lin‖lin configuration, focusing our attention to the signal between ground-state Zeeman sublevels, such as $m_F=\pm 1$, which is a good candidate for compact and high performance atomic clocks. This interaction scheme is characterized by quantum interference between dark states prepared through the two excited hyperfine states. A model is developed taking into account the multilevel structure of the atomic system and the linewidth of the lasers. We study the signal as a function of the laser detuning, i.e., the excited-state hyperfine structure. By comparing the model and the experimental results, we can quantify the influence of each dark state on the lin‖lin CPT resonance. Finally, the good quantitative agreement between theory and experiments allows predicting the effects of the laser linewidth on the lin‖lin CPT resonance.

ACKNOWLEDGMENTS

[1] K. Takagi, R. F. Curl, and R. T. M. Su, Appl. Phys. **7**, 181 (1975).

[2] G. Alzetta, A. Gozzini, M. Moi, and G. Orriolis, Nuovo Cimento Soc. Ital. Fis., B **36**, 5 (1976).

[3] E. Arimondo and G. Orriols, Lett. Nuovo Cimento Soc. Ital. Fis. **17**, 333 (1976).

[4] S. E. Harris, Phys. Today **50**(7), 36 (1997).

[5] A. Lezama, S. Barreiro, and A. M. Akulshin, Phys. Rev. A **59**, 4732 (1999).

[6] A. Nagel, K. Graf, A. Naumov, E. Mariotti, V. Biancalana, D. Meschede, and R. Wynands, Europhys. Lett. **44**, 31 (1998).

[7] J. Vanier, Appl. Phys. B: Lasers Opt. **81**, 421 (2005).

[8] L. V. Hau, S. E. Harris, Z. Dutton, and C. H. Behroozi, Nature **397**, 594 (1999); G. P. Djotyan, Opt. Express **4**, 113 (1999).

[9] M. Rosenbluh, V. Shah, S. Knappe, and J. Kitching, Opt. Express **14**, 6588 (2006).

[10] J. Kitching, L. Hollberg, A. V. Taichenachev, V. L. Velichan-sky, and V. I. Yudin, Laser Phys. Lett. **1**, 257 (2004).

[11] G. A. Kazakov *et al.*, Eur. Phys. J. D **35**, 445 (2005).

[12] A. B. Post, Y.-Y. Jau, N. N. Kuzma, and W. Happer, Phys. Rev. A **72**, 033417 (2005).

[13] T. Zanon, S. Guerandel, E. de Clercq, D. Holleville, N. Dimarcq, and A. Clairon, Phys. Rev. Lett. **94**, 193002 (2005).

[14] G. Kazakov, B. Matisov, I. Mazets, G. Mileti, and J. Delporte, Phys. Rev. A **72**, 063408 (2005).

[15] A. V. Taichenachev, V. I. Yudin, V. L. Velichansky, and S. A. Zibrov, Pis'ma Zh. Eksp. Teor. Fiz. **82**, 449 (2005).

[16] R. Wynands, A. Nagel, S. Brandt, D. Meschede, and A. Weis, Phys. Rev. A **58**, 196 (1998).

[17] S. Knappe, M. Stähler, C. Affolderbach, A. V. Taichenachev, V. I. Yudin and R. Wynands, Appl. Phys. B: Lasers Opt. **76**, 57 (2003).

[18] M. D. Lukin, S. F. Yelin, M. Fleischhauer, and M. O. Scully, Phys. Rev. A **60**, 3225 (1999).

[19] D. V. Kosachiov, B. G. Matisov, and Yu. V. Rozhdestvensky, J. Phys. B **25**, 2473 (1992).

[20] E. A. Korsunsky, N. Leinfellner, A. Huss, S. Baluschev, and L. Windholz, Phys. Rev. A **59**, 2302 (1999).

[21] C. Affolderbach, S. Knappe, R. Wynands, A. V. Tavichenachev, and V. I. Yudin, Phys. Rev. A **65**, 043810 (2002).

[22] M. J. McDonnell, D. N. Stacey, and A. M. Steane, Phys. Rev. A **70**, 053802 (2004).

[23] D. D. Yavuz, Phys. Rev. A **75**, 031801 (2007).

[24] S. Knappe, P. Schwindt, V. Shah, L. Holberg, J. KitchingL. Liew, and J. Moreland, Opt. Express **13**, 1249 (2005) .

[25] E. Breschi, G. Kazakov, R. Lammegger, B. Matisov, L. Windholz, and G. Mileti, IEEE Trans. Ultrason. Ferroelectr. Freq. Control **56**, 926 (2009).

[26] G. A. Kazakov, B. G. Matisov, I. E. Mazets, and Yu. V. Rozhdestvensky, Tech. Phys. **51**, 1414 (2006).

[27] A. V. Taĭchenachev, V. I. Yudin, R. Wynands, M. Stahler, J. Kitching, and L. Hollberg, Phys. Rev. A **67**, 033810 (2003).

[28] D. V. Kosachev, Quantum Electron. **25**, 1089 (1995).

[29] P. Violino, Nuovo Cimento A **6**, 440 (1968).

[30] I. E. Mazets and B. G. Matisov, Sov. Phys. JETP **74**, 13 (1992).

[31] D. A. Varshalovich, A. N. Moskalev, and V. K. Khersonskii, *Quantum Theory of Angular Momentum* (World Scientific, Singapore, 1988).

[32] L. D. Landau and E. M. Lifshitz, *Quantum Mechanics, Non-Relativistic Theory* (Pergamon, Oxford, 1991), Vol. 3.

[33] R. H. Dicke, Phys. Rev. **89**, 472 (1953).

[34] C. Affolderbach, A. Nagel, S. Knappe, C. Jung, D. Wiedenmann, and R. Wynands, Appl. Phys. B **70**, 407 (2000).

[35] DF-DAVLL is acronym of Doppler-free dichroich atomic vapor laser locking.

[36] G. Wasik, W. Gawlik, J. Zachorowski, and W. Zawadzki, Appl. Phys. B: Lasers Opt. **75**, 613 (2002).

[37] B. J. Dalton and P. L. Knight, J. Phys B **15**, 3997 (1982).

[38] A_C is proportional to the variation in the transmitted laser power through the cell relative to a constant background.

[39] M. V. Romalis, E. Miron, and G. D. Cates, Phys. Rev. A **56**, 4569 (1997).

[40] W. Happer and S. Mathur, Phys. Rev. **163**, 12 (1967).

[41] J. E. Bjorkholm and P. F. Liao, Phys. Rev. Lett. **33**, 128 (1974).

[42] A. Nagel, C. Affolderbach, S. Knappe, and R. Wynands, Phys. Rev. A **61**, 012504 (1999).

[43] N. Beverini, P. Minguzzi, and F. Strumia, Phys. Rev. A **4**, 550 (1971).